Toxicology and Applied Pharmacology 254 (2011) 299–310

Contents lists available at ScienceDirect

Toxicology and Applied Pharmacology

journal homepage: www.elsevier.com/locate/ytaap

The aryl hydrocarbon receptor interacts with ATP5α1, a subunit of the ATP synthase complex, and modulates mitochondrial function

Dorothy M. Tappenden [a,b], Scott G. Lynn [a,b], Robert B. Crawford [c], KangAe Lee [a], Ajith Vengellur [a], Norbert E. Kaminski [b,c], Russell S. Thomas [e], John J. LaPres [a,b,d,*]

[a] Department of Biochemistry and Molecular Biology, Michigan State University, East Lansing, MI 48824-1319, USA
[b] Center for Integrative Toxicology, Michigan State University, East Lansing, MI 48824-1319, USA
[c] Department of Pharmacology and Toxicology, Michigan State University, East Lansing, MI 48824-1319, USA
[d] Center for Mitochondrial Science and Medicine, Michigan State University, East Lansing, MI 48824-1319, USA
[e] The Hamner Institutes for Health Sciences, Research Triangle Park, NC 27709, USA

ARTICLE INFO

Article history:
Received 1 March 2011
Revised 28 April 2011
Accepted 4 May 2011
Available online 12 May 2011

Keywords:
Aryl hydrocarbon receptor
Dioxin
Mitochondria
ATP synthase
ATP5a1

ABSTRACT

Dioxins, including 2,3,7,8 tetrachlorodibenzo-*p*-dioxin (TCDD), produce a wide range of toxic effects in mammals. Most, if not all, of these toxic effects are regulated by the aryl hydrocarbon receptor (AHR). The AHR is a ligand activated transcription factor that has been shown to interact with numerous proteins capable of influencing the receptor's function. The ability of secondary proteins to alter AHR-mediated transcriptional events, a necessary step for toxicity, led us to determine whether additional interacting proteins could be identified. To this end, we have employed tandem affinity purification (TAP) of the AHR in Hepa1c1c7 cells. TAP of the AHR, followed by mass spectrometry (MS) identified ATP5α1, a subunit of the ATP synthase complex, as a strong AHR interactor in the absence of ligand. The interaction was lost upon exposure to TCDD. The association was confirmed by co-immunoprecipitation in multiple cell lines. In addition, cell fractionation experiments showed that a fraction of the AHR is found in the mitochondria. To ascribe a potential functional role to the AHR:ATP5α1 interaction, TCDD was shown to induce a hyperpolarization of the mitochondrial membrane in an AHR-dependent and transcription-independent manner. These results suggest that a fraction of the total cellular AHR pool is localized to the mitochondria and contributes to the organelle's homeostasis.

Introduction

2,3,7,8 tetrachlordibenzo-*p*-dioxin (TCDD) is a prototypical dioxin and a member of the halogenated aromatic hydrocarbons (HAH) (Poland and Glover, 1980; Bradfield and Poland, 1988; Mandal, 2005). Dioxins are pervasive, being found in soil and at every level of the food chain (Kearney et al., 1973; Poland and Knutson, 1982). These compounds are highly stable, lipophilic molecules that induce a battery of toxic endpoints in mammals (Poland et al., 1979). Among the adverse effects attributed to dioxin exposure are compromised immune system responses, wasting disease, hyperplasia of the liver, birth defects, metabolic syndrome, and an increased risk of diabetes and cancer (Schmidt and Bradfield, 1996; Mandal, 2005). The cellular mechanisms that govern these toxic endpoints have not yet been fully elucidated; however; most, if not all, involve the aryl hydrocarbon receptor (AHR).

TCDD and other planar HAHs have been characterized as exogenous ligands for the AHR (Poland et al., 1976; Poland and Glover, 1977). In the absence of ligand, the AHR is found in the cytosol, complexed with the aryl-hydrocarbon receptor associated protein nine (ARA9, also known as XAP2 and AIP), and a homodimer of heat shock protein 90 (Hsp90) (Perdew, 1988; Carver et al., 1998). Upon ligand binding, the AHR translocates into the nucleus, and becomes an active transcription factor via heterodimerization with the aryl hydrocarbon receptor nuclear translocator (ARNT) (Prokipcak et al., 1990). The AHR/ARNT dimer binds to xenobiotic response element (XRE) regions of DNA to regulate gene expression (Fujisawa-Sehara et al., 1987; Denison et al., 1988). XREs are found in a wide battery of genes, including those that encode cytochrome P450s, such as *CYP1A1*, the canonical marker of dioxin exposure (Poland and Kende, 1977). Though AHR-regulated gene expression is necessary for toxicity, a complete understanding of the relationship between AHR cellular signaling, gene regulation, and the pleiotropic toxicity observed in dioxin exposure has not been achieved.

The AHR cytosolic complex has been previously reported to influence a host of proteins that are intimately involved with cell cycle, cellular homeostasis, mitochondrial function, disease, and cell death (Schmidt and Bradfield, 1996; Tian et al., 2002; Barhoover et al., 2009). The objective of the present investigation was to identify novel protein interactions with the AHR using tandem affinity purification (TAP) and mass spectrometry (MS). Using this approach, a physical

* Corresponding author at: Department of Biochemistry and Molecular Biology, Michigan State University, East Lansing, MI 48824-1319, USA. Fax: +1 517 353 9334.
E-mail address: lapres@msu.edu (J.J. LaPres).

0041-008X/$ – see front matter © 2011 Elsevier Inc. All rights reserved.
doi:10.1016/j.taap.2011.05.004

interaction between the AHR and ATP5α1, a subunit of the ATP synthase complex, was demonstrated. The AHR/ATP5α1 interaction was further verified by co-immunoprecipitation followed by Western blotting and cellular fractionation studies which also identified the AHR in the mitochondria. Interestingly, TCDD treatment of several different cell lines that vary in their level of AHR expression demonstrated a hyperpolarization of the mitochondrial inner membrane that was only observed in AHR expressing cells. Although the physiological role of the AHR within the mitochondria compartment is not fully understood, it is tempting to speculate that the metabolic disorders, including the enigmatic wasting syndrome, produced in some animal species by TCDD may be, in part, related to disruption of AHR function within the mitochondria. Collectively our findings suggest that the AHR plays a direct role in mitochondrial function and cellular energetics through protein–protein interactions with ATP5α1.

Materials and methods

Materials. Oligonucleotide synthesis was performed at Macromolecule Synthesis Facility at Michigan State University. pTarget and pGEM-T Easy vectors were obtained from Promega (Madison, WI). The pZome1C vector was obtained from Cellzome (Cambridge, UK). The Phoenix-eco cell line was a generous gift from Dr. Garry Nolan (Stanford University, Palo Alto, CA) and the AHR−/− mouse embryonic fibroblast cell line and rabbit polyclonal anti-AHR BEAR3 were generous gifts from Dr. Christopher Bradfield (University of Wisconsin-Madison). The other antibodies used were obtained from the following sources: mouse monoclonal anti-ATP5α1 (cat #ab14748) and rabbit polyclonal anti-Hsp90 (cat #ab19021) were obtained from Abcam (Cambridge, MA), mouse monoclonal anti-COXIV (cat #A21349) was obtained from Invitrogen, and rabbit anti-LDH was a generous gift from Dr. John Wang (Michigan State University). Goat polyclonal anti-SODII (cat #sc18503), donkey anti-goat (cat #sc2033), goat-anti rabbit (cat # sc2004) and mouse (cat #sc2005), normal mouse IgG (cat #sc2025) and protein G resin were purchased from Santa Cruz Biotechnology (Santa Cruz, CA). Monoclonal mouse anti-rabbit IgG, light chain specific, DyLight 488 conjugated (cat #211-482-171) and goat anti-mouse IgG, light chain specific, DyLight 594 conjugated (cat#151-515-174) were obtained from Jackson Immunoresearch (West Grove, PA). Protease inhibitor tablets (cat #11836170001) were purchased from Roche (Indianapolis, IN). All other chemicals were reagent grade and purchased from Sigma Aldrich (St. Louis, MO).

Plasmids. The cDNAs for the murine AHR and green fluorescent protein (GFP) were amplified using the following primers: AHR: 5′-ggatccccaccatgagcagcggcgccaacatcacc-3′ and 5′-ggatcctgcactctgcaccttgcttagg-3′ GFP: 5′-gggggatccaccatggtgagcaagggcgac-3′ and 5′-gtggatccccgggcccgcggtaccgtcgactgc-3′ The amplicons were cloned into p-Target and pGEM-T Easy, respectively. Each cDNA was subcloned into pZome1C vector. Use of the pZome1C vector places the TAP-tag at the C terminal of both the AHR and GFP gene. Clones were isolated with ampicillin selection and sequence verified.

Cell culture and dosing regime. The Phoenix-eco and Hepa1c1c7 cells were maintained in DMEM with L-glutamine and supplemented with 10% cosmic calf serum, 100 units/mL penicillin, 100 μg/mL streptomycin, and 1 mM sodium pyruvate. Hepa C12 cells were maintained in DMEM with L-glutamine and supplemented with 10% cosmic calf serum and 1 mM sodium pyruvate. Tissue culture media and supplements were purchased from Invitrogen (Carlsbad, CA) and cosmic calf serum was purchased from HyClone (Waltman, MA). Hepa1c1c7 TAP-AHR and TAP-GFP were grown in the above media, supplemented with puromycin (2 μg/mL) (US Biological, Swampscott, MA). The AHR−/− mouse embryonic fibroblast (MEF) cell line was maintained in DMEM with L-glutamine and supplemented with 10% fetal calf serum, 100 units/mL penicillin, 100 μg/mL streptomycin, 1 mM sodium pyruvate, and 1× non-essential amino acids. AHR−/− MEF cell lines with TAP-AHR or TAP-GFP were grown in the above media and supplemented with puromycin (3 μg/mL). The CH12.LX B cell line derived from the murine CH12 B-cell lymphoma (Arnold et al., 1983), which arose in B10.H-2^{a}H-4^{b}p/Wts mice (B10.A×B10.129), has been previously characterized by Bishop and Haughton (1986) and was a generous gift from Dr. Geoffrey Haughton (University of North Carolina). The BCL-1 B-cell line was derived from a murine B-cell lymphoma that spontaneously arose in a BALB/c mouse (Slavin and Strober, 1978) and was generously provided by Dr. Kathryn H. Brooks (Michigan State University). CH12.LX and BCL-1 cells are mature B cells (surface Ig^{+}) and were grown in RPMI-1640 (Gibco BRL, Grand Island, NY) supplemented with heat-inactivated 10% bovine calf serum (Hyclone, Logan, UT), 13.5 mM HEPES, 23.8 mM sodium bicarbonate, 100 units/mL penicillin, 100 μg/mL streptomycin, 2 mM L-glutamine, 0.1 mM non-essential amino acids, 1.0 mM sodium pyruvate, and 50 μM b-mercaptoethanol. Cells were maintained at 37 °C in an atmosphere of 5% CO_2.

Transfection/stable cell line infection. The TAP-AHR and TAP-GFP retroviral vectors were transfected into Phoenix-eco (P-eco) cells for packaging using Lipofectamine (Invitrogen) via manufacturer's instructions. After the initial incubation (5 to 8 h, 37 °C) in the presence of DNA, the media was removed and replaced with Phoenix cell growth media containing chloroquine (25 μM). Cells were incubated for 24 h (37 °C) and media was replaced with fresh Phoenix cell growth media and incubated for an additional 24 h (32 °C). Cellular debris was removed from the media by centrifugation (3 min, 67*g*, in RT7, Sorvall, Rockford, IL), and purified by filtration through a 0.45 μm membrane filter (Millipore, Billerica, MA). Hepa1c1c7 wild type and MEF AHR−/− target cell lines were exposed to this virus containing media for 3 h at 32 °C and 5% CO_2. After this incubation, Hepa media containing 15 μg/mL polybrene was added and target cells were incubated for 24 h (32 °C). Media was replaced and the target cells were cultured at 37 °C to approximately 80% confluence. Cells were then passaged and selected using Hepa media containing 2 μg/mL puromycin.

Western blot analysis. Total protein samples were prepared and concentrations determined as previously described (Lowry et al., 1951; Lee et al., 2006). Proteins were separated on 4–12% Nu-Page Bis-Tris gels (Invitrogen), transferred to nitrocellulose membranes, and probed with various antibodies as previously described (Vengellur and LaPres, 2004). Westerns blots were visualized using ECL Western blotting substrate (Pierce, Rockford, IL)

Quantitative real-time PCR analysis. The AHR-TAP and GFP-TAP MEF AHR−/− cell lines were used for functional analysis of the TAP-AHR. *CYP1A1* gene expression was examined after exposure to vehicle (0.01% dimethyl sulfoxide, DMSO) or TCDD (10 nM) for 6 h. Total RNA was extracted from the cells using TRIzol (Invitrogen) per manufacturer's protocol. RNA concentrations were determined by UV spectrophotometry (Nanodrop, Wilminton, DE). Total RNA (1 μg) was reverse-transcribed using anchored oligo $(dT)_{18}$ primers and M-MLV reverse transcriptase (Invitrogen). Reactions were carried out according to manufacturer's protocol. CYP1A1 gene expression was measured by quantitative real-time PCR (qRT-PCR) using the SYBR-Green system and an ABI PRISM 7000 Sequence Detection System (Applied Biosystems, Foster City, CA) (Vengellur and LaPres, 2004). The primers used were: CYP1A1, 5′-AAGTGCAGATGCGGTCTTCT-3′ and 5′-AAAGTAGGAGGCAGGCACAA-3′; Hypoxanthine-guanine phosphoribosyltransferase (HGPRT) 5′-AAGCCTAAGATGAGCGCAAG-3′ and 3′-TTACTAGGCAGATGGCCACA-5′.

Tandem affinity purification. Approximately 2.5×10^9 Hepa1c1c7 TAP-AHR and TAP-GFP cell were treated with vehicle (0.01% DMSO) or TCDD (10 nM) for 30, 120, or 240 min. Dosing media was removed and cells were washed three times with phosphate buffered saline (PBS) and harvested in TAP-tag lysis buffer (TTLB) (5% glycerol, 50 mM Tris, pH 7.5, 50 mM $MgCl_2$, 100 mM NaCl, 0.1% NP40, 1 mM dithiothreitol (DTT), 1 mM Na_3VO_4, 25 mM NaF, protease inhibitor tablets). Cells were disrupted by two cycles of freeze/thaw, and insoluble material was removed by centrifugation (7000*g*, 20 min). Samples were then incubated with 200 μL of IgG Sepharose beads (GE Healthcare, Waukesha, WI) for 4 h, at 4 °C with rotation. Beads were collected by centrifugation (45*g*, 30 s) and transferred to Poly-Prep Chromatography columns (BioRad, Hercules, CA). Columns were extensively washed with TTLB, followed by washing with tobacco etch virus (TEV) cleavage buffer (10 mM Tris, pH 7.5, 150 mM NaCl, 0.1% NP40, 0.5 mM EDTA, 1 mM DTT). Beads were incubated (18 h, 4 °C) in 1.5 mL TEV cleavage buffer containing AcTEV protease (Invitrogen) (450 units). Eluates were collected by gravity flow. IgG sepharose resin was washed with 1.5 mL of TEV buffer and 9 mL of calmodulin binding buffer (CBB) (10 mM β-mercaptoethanol, 10 mM Tris, pH 7.5, 150 mM NaCl, 1 mM MgOAc, 1 mM imidazole, 0.1% NP40, 2 mM DTT). Washes were combined with eluate. Samples were then incubated with 200 μL calmodulin affinity resin (Stratagene, La Jolla, CA) (4 h, 4 °C). Calmodulin resin was transferred to new Ploy-Prep Chromatography columns, supernatant was removed and resin was washed extensively with CBB. Warm 3× sodium dodecyl sulfate (SDS) buffer (4.8% SDS, 100 mM Tris pH 6.8, 16% glycerol, 8% β-mercaptoethanol, 0.4% bromophenol blue) was added to resin to remove protein complexes.

Gel electrophoresis and mass spectrometry. Samples were separated on a 4–12% Bis-Tris gradient gel (NuPage, Invitrogen) by electrophoresis. Gels were silver stained using SilverSNAP staining kit (Pierce, Rockford, IL) according to manufacturer's protocol and the gel was photographed. Specific bands were excised from the matrix and destained with SilverSNAP destaining kit and subjected to in-gel tryptic digestion as previously described (Shevchenko et al., 1996). The extracted peptides were then automatically injected by a Waters nanoAcquity Sample Manager (Milford, MA) loaded for 5 min onto a Waters Symmetry C18 peptide trap (5 μm, 180 μm×20 mm) at 4 μL/min in 5% acetonitrile /0.1% formic acid. The bound peptides were then eluted onto a Waters BEH C18 nanoAcquity column (1.7 μm, 100 μm×100 mm) over 35 min with a gradient of 2% B to 35% B in 21 min, 90% B from 21–24 min and back to constant 5% B at 24.1 min using a Waters nanoAcquity UPLC (Buffer A = 99.9% Water/0.1% Formic Acid, Buffer B = 99.9% Acetonitrile/0.1% Formic Acid) with an initial flow rate of 600 nL/min, ramping to 700 nL/min at 80 min and back to 600 nL/min at 86 min. Eluted peptides were sprayed into a ThermoFisher LTQ Linear Ion trap mass spectrometer outfitted with a MICHROM Bioresources ADVANCE nano-spray source. The top five ions in each survey scan were then subjected to data-dependant zoom scans followed by low energy collision induced dissociation (CID) and the resulting MS/MS spectra were converted to peak lists using BioWorks Browser v 3.3.1 (ThermoFisher, Rockford, IL) using the default LTQ instrument parameters. Peak lists were searched against all mouse sequences available in the NCBI nr database, downloaded on 11-16-2008 from NCBI, using the Mascot searching algorithm, v2.2 (www.matrixscience.com). The Mascot output was then analyzed using Scaffold (www.proteomesoftware.com) to probabilistically validate protein identifications using the ProteinProphet computer algorithm. Assignments validated above the Scaffold 95% confidence filter are considered true.

Co-immunoprecipitation. Hepa1c1c7 and CH12.LX wild type cells were grown to confluence, washed with cold PBS and harvested in TAP-tag lysis buffer. Equal amounts of the Hepa1c17 and CH12.LX cellular supernatant were incubated with 2 μg/μL of normal mouse IgG or ATP5α1 antibody for 90 min and then Protein G beads (30 μL) were added to the samples and incubated for an additional 90 min. The supernatant was removed and the beads were washed in TAP-tag lysis buffer. Samples were eluted from the beads using 3× SDS buffer and separated by Nu-PAGE Bis-Tris 4–12% gradient gel matrix, transferred to nitrocellulose membrane, and probed with primary AHR antibody.

Cellular fractionation. Hepa1c1c7 wild type cells were grown to near confluence and then treated with vehicle (0.01% DMSO) or TCDD (10 nM) for 2 h. Cells were harvested in fractionation buffer (25 mM sucrose, 20 mM Tris–HCl, 1 mM EDTA, pH7.4) and dounce homogenized (100 stokes). An aliquot of this was taken as the whole cell lysates (WLC) fraction. CH12.LX cells were harvested in fractionation buffer and dounce homogenized, as above. Liver tissue was homogenized with Tissue-Tearor (Biospec, Bartlesville, OK) in fractionation buffer and then dounce homogenized, as above. Insoluble materials were removed by centrifugation (400*g*, 10 min) and the supernatant was transferred to a new tube. The supernatant and organelle fractions were separated by centrifugation (4500*g*, 10 min). The supernatant was removed and the organelle pellet was resuspended in 1 mL of fractionation buffer and dounce homogenized (14–20 strokes). An aliquot of the supernatant was taken as the cytosolic fraction (Cyto) and an aliquot of the pellet after resuspension and homogenization was taken as the impure mitochondrial fraction (MF1). Large debris was removed by centrifugation (400*g*, 10 min), the supernatant was transferred to a new tube and mitochondria were collected by centrifugation (4500*g*, 10 min). The isolated mitochondrial pellet was resuspended in 250 μL fractionation buffer and is the pure mitochondrial fraction (MF2). Mitoplasts were prepared using osmotic shock as previously described with minor modifications (Daum et al., 1982). The purified mitochondria pellet was resuspended in mitoplast buffer (4.2 mM sucrose, 20 mM Tris–HCl, 1 mM EDTA, pH 7.4) and incubated on ice, for 20 min. Large debris was again removed by centrifugation (400*g*, 10 min), the supernatant was transferred to a new tube and mitoplasts were collected by centrifugation (4500*g*, 20 min). Supernatant was collected and is inner membrane space fraction (MF3). The pellet was resuspended in 100 μL fractionation buffer and is the isolated mitochondrial inner membrane fraction (MF4).

Immunohistochemistry. Hepa1c1c7 wild type cell were grown to 80% confluence and mitochondria were isolate as described above. Isolated mitochondria were resuspended in 150 μL of mitochondria buffer and 20 μL were placed on glass slide. Mitochondria were fixed in methanol/acetone (1:1 v/v, 20 min, −20 °C). Samples were allowed to air dry at room temperature. Primary antibodies for AHR and ATP5α1 were diluted 1:10,000 in a 1% BSA PBS solution, added to samples and incubated overnight at 4 °C. Samples were washed 3× with ice cold PBS. Secondary Immunofluorescence antibodies were diluted 1:5000 in a 1% BSA in PBS, added to samples, and incubated for 20 min at 4 °C. Samples were washed with ice cold PBS. A glass cover slip was placed onto the samples and stored in the dark until imaging. Images were captured using an Olympus FluoView FV1000 (Olympus America, Inc, Center Valley, PA) configured on a fully automated IX81 inverted microscope at the Center for Advanced Microscopy, Michigan State University.

Mitochondrial inner membrane potential determination. CH12.LX and BCL-1 cells were grown in cell type appropriate media to a concentration of 1×10^6 cells/mL. Cells were then transferred into a 96 well culture plate at 1×10^5 cells per well. The culture plates were immediately centrifuged at 300*g* for 5 min (24 °C), media was decanted and culture plates were gently agitated to disperse the cell pellet. Replicate wells (8 replicates per treatment) were then exposed to control media, vehicle (0.01%, DMSO), carbonyl cyanide m-chlorophenylhydrazone (CCCP, 12.5 μM), or TCDD (3, 10, or 30 nM) for 6 h. Cells were exposed to mitomycin C where

indicated. Culture plates were centrifuged as above, treatment media was decanted and 4 wells per treatment were exposed to 100 μL of high glucose normal buffer (HGNB, 130 mM NaCl, 5.5 mM KCl, 1.8 mM $CaCl_2$, 1.0 mM $MgCl_2$, 25 mM glucose, 20 mM HEPES, pH 7.4) with either 500 nM tetramethylrhodamine methyl ester (TMRM) or 250 nM MitoTracker Green (MTG) for 30 min. Culture plates were then centrifuged, decanted, agitated, and cells were resuspended in 150 μL of HGNB. This procedure was repeated two more times and then the culture plates were analyzed by flow cytometry (FCM). Hepa1c17 and Hepa C12 cells were grown to 70% confluence and dosed with vehicle or TCDD for 6 h. Media were removed and the cells were exposed to TMRM or MTG for 30 min in HGNB. Cells were then trypsinized, washed as above, and analyzed by FCM. Events, 35,000, were recorded per well on a BD FACSCanto II (BD Biosciences, San Jose, CA). Singlet gating was applied and the mean fluorescence intensity (MFI) for both TMRM and MTG fluorescence per cell was calculated for each well and then the average MTG across replicates was determined within a treatment group. Average TMRM per well was divided by average MTG per well per treatment to generate TMRM/MTG fluorescence.

ATP determination. CH12.LX cells were seeded at 8×10^5 cells/well in a 6 well culture plate and grown to ~80% confluence. The cells were then treated with vehicle (0.01%, DMSO) or TCDD (10 nM) for 6 h. An aliquot of each sample was taken for cell counts. Samples were then precipitated with 1 N perchloric acid, centrifuged (13,000*g*, 15 min) to pellet cellular debris, aqueous sample was then neutralized with equal volume of 1 N NaOH. ATP levels were measured using ATP determination kit (Invitrogen) according to manufacturer's protocol.

Results

AHR-TAP and GFP-TAP tagged cell line expression and function

AHR−/− MEFs expressing AHR-TAP and GFP-TAP were created and tested for proper expression and function. Western blot analysis showed that the TAP-tagged versions of both proteins were expressed at high levels in the MEFs and Hepa1c1c7 cells (Fig. 1A and B). In addition, the transduced AHR-TAP protein was capable of rescuing dioxin-induced CYP1A1 expression in the AHR−/− MEF cell line (Fig. 1C). The expression of the AHR-TAP protein in the MEF cell line did not remain stable; therefore, AHR-TAP and GFP-TAP genes were transduced into wild type Hepa1c1c7 cells (Fig. 1B). It is hypothesized that the loss of stable expression of the AHR-TAP in the AHR−/− MEFs explains the decrease in TCDD-induced Cyp1A1 expression; however, a modest inhibition of the transactivation domain due to the TAP-tag cannot be ruled out.

Identification of AHR complex proteins

Initially, the AHR-TAP and GFP-TAP expressing Hepa1c1c7 cell strains were used to verify the specificity of known AHR-interacting proteins, Hsp90 and ARA9. TAP of the AHR, followed by MS identified the AHR, Hsp90, ARA9, and ARNT at the correct molecular weights only in the AHR-TAP expressing cells (Fig. 2A). Hsp90 and ARA9 were identified with greater than 95% confidence using MASCOT and Scaffold data analysis software and ARNT was identified consistently, but with less confidence (Fig. 2B). In the TCDD (10 nM) dosed time course experiment data sets, these protein interactions were decreased, in accordance with disassociation of the AHR from its cytosolic complex in

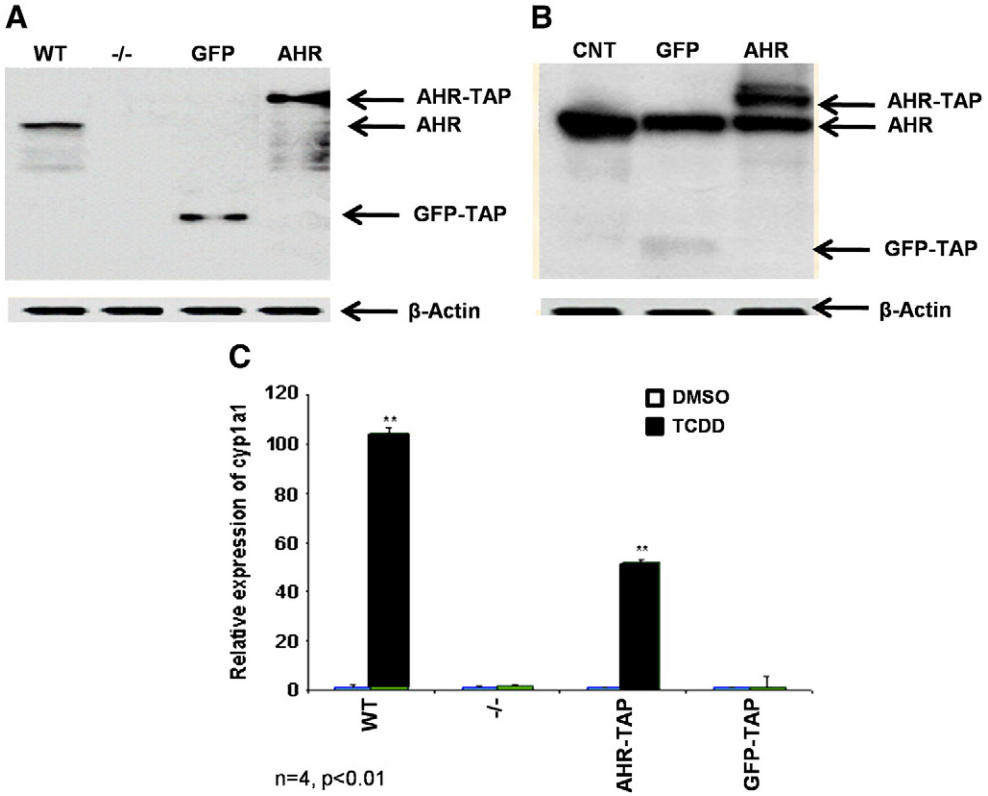

Fig. 1. Western blot analysis using an AHR specific antibody was performed to confirm protein expression. Cell strains expressing TAP-tagged GFP (GFP-TAP) or murine AHR (AHR-TAP) were established in AHR null (−/−) MEFs. AHR +/+ (WT) MEFs are included as a positive control (A). GFP-TAP and AHR-TAP were also expressed in Hepa1c1c7 cells. The parental Hepa1c1c7 cells are included as a negative control (CNT). β-actin was used as a loading control (B). Functional activity of AHR-TAP (C) was determined by qRT-PCR of Cyp1A1 induction in wild type (WT), AHR−/− (−/−), AHR−/− expressing AHR-TAP, and AHR−/− expressing GFP-TAP MEFs. Cell strains were exposed to DMSO (0.01% vehicle control) and TCDD (10nM) for 6 h, RNA was isolated and quantified for Cyp1A1 levels using SYBR green. Cyp1A1 levels were normalized to HPRT. $^*p<0.05$ when compared to DMSO treated cells within the same cell line.

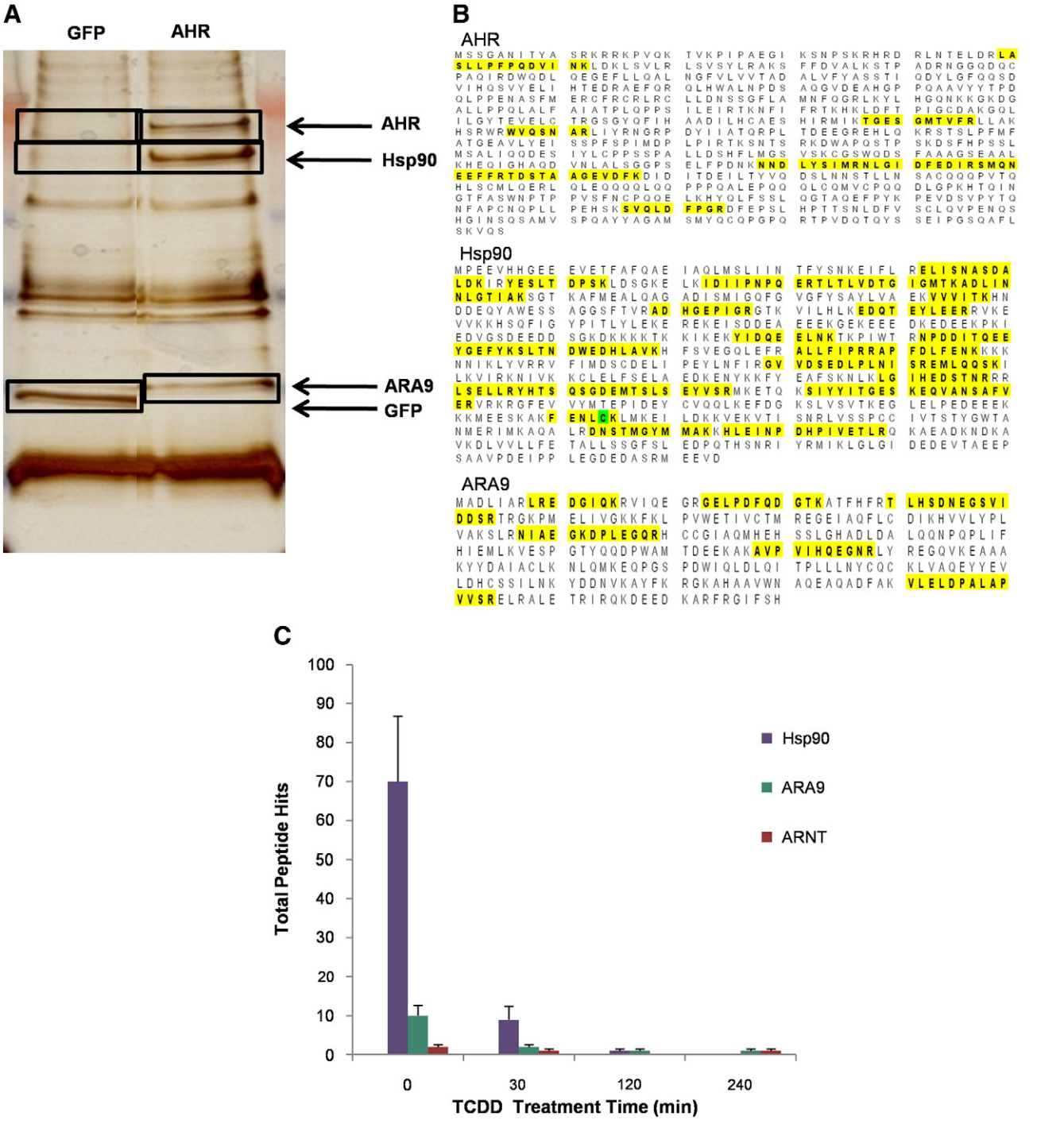

Fig. 2. Silver stain gel of TAP samples. The final TAP elute samples of AHR-TAP and GFP-TAP Hepa1c1c7 were separated on a 4–12% gradient SDS-Page gel and visualized using silver stain (A). Gel slices (black boxes) were analyzed as described in Materials and methods. (B) MS identification of AHR and cytosolic complex proteins Hsp90 and ARA9. Highlighted regions show identified peptide sequences. All were identified at a >95% confidence using the ProteinProfit algorithm. (C) Total numbers of peptides identified by mass spectrometry of known interactors following TAP of the AHR.

the presence of ligand (Fig. 2C). ARNT was also identified in three of four time points including the 240 min sample. The number of ARNT peptides identified was modest compared to Hsp90 and ARA9. This apparent lack of affinity is attributed to the transient nature of the AHR–ARNT interaction and TCDD-induced degradation of the AHR.

Identification of ATP5α1 protein interaction with the AHR

A novel interaction between the AHR and ATP5α1 was identified by TAP/MS method (Fig. 3A). ATP5α1, a catalytic subunit of ATP synthase, was identified at a confidence level of greater than 95% using the MASCOT and Scaffold analysis software (Fig. 3B). Western blot analysis of the purified AHR complex, after TAP, confirmed the identity of ATP5α1 (Fig. 4A). The interaction between the AHR and ATP5α1 was lost upon TCDD treatment (10 nM, 120 min), suggesting that activation of the AHR leads to its dissociation from the ATP synthase complex (Fig. 4A). Given that the AHR:ATP5α1 interaction was identified using an ectopic expression system, co-immunoprecipitation from wild type Hepa1c1c7 cells was performed. The AHR:ATP5α1 interaction was further confirmed at endogenous protein

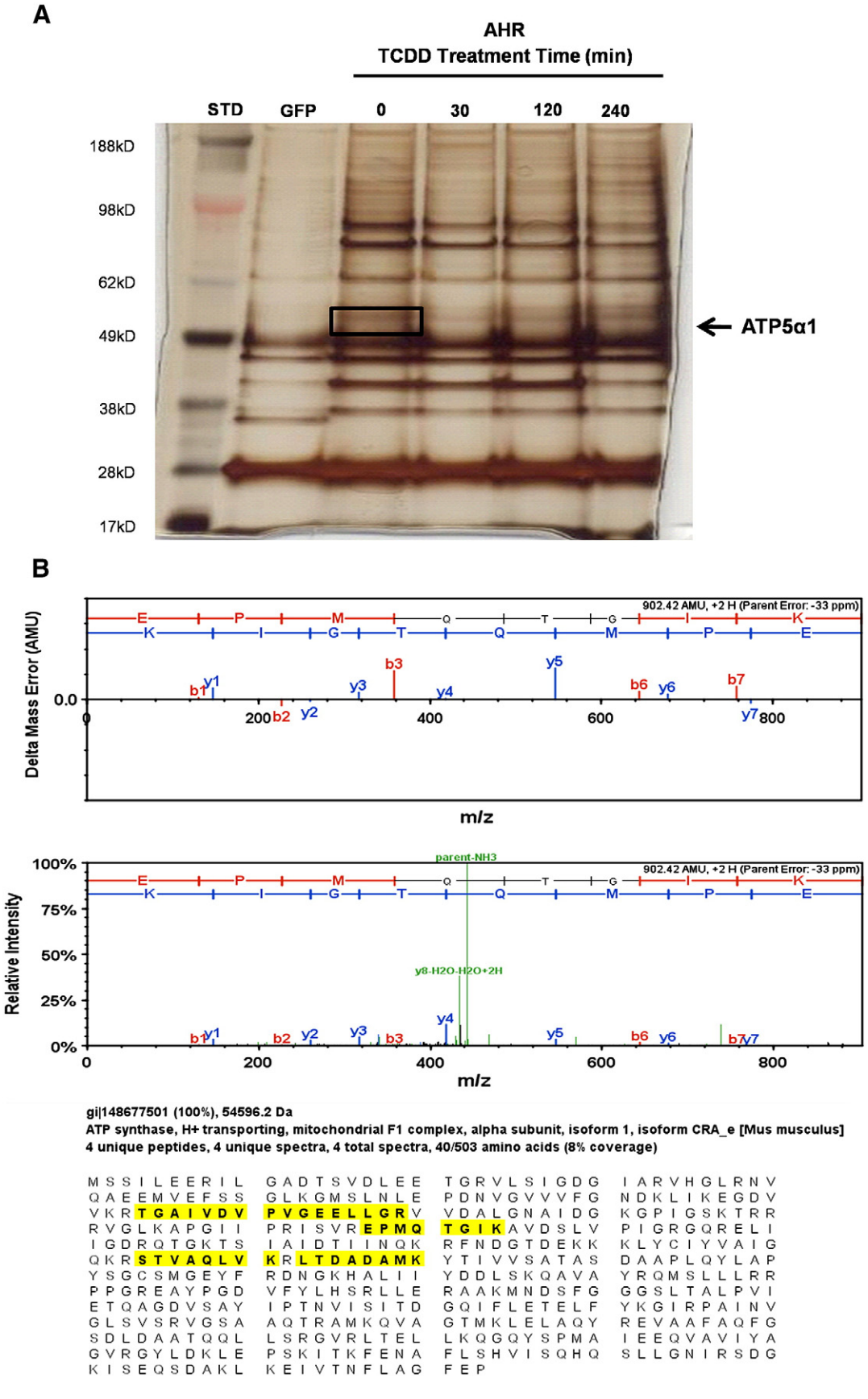

Fig. 3. Silver stained gel of TCDD time course experiment, lanes represent GFP-TAP, AHR-TAP (no dose, 30, 120, 240 min) 10nM TCDD exposure. Black box denotes gel slice from which ATP5α1 was only one of the identified proteins (A). ATP5α1 mass spectrometry data following AHR TAP, including error probability, signal intensity measurements and peptide sequence coverage (highlighted) aligned to the protein sequence (B).

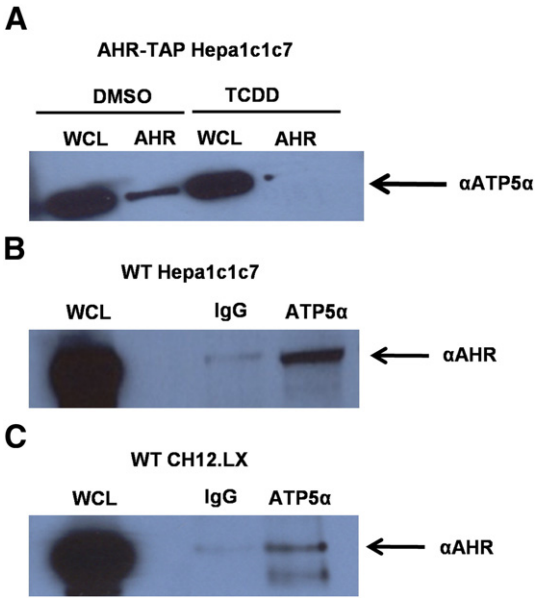

Fig. 4. Co-Immunoprecipitation of the AHR and ATP5α1. Extracts from DMSO (0.01% vehicle control) or TCDD treated (10 nM, 120 min) AHR-TAP Hepa1c1c7 cells under went TAP purification. The resulting precipitate was separated by gel electrophoresis. Western blotting was performed and probed with an ATP5α1 specific antibody (A). Extracts from WT Hepa1c17 (B) or CH12.LX (C) were immunoprecipitated with an ATP5α1 specific antibody or IgG control. Protein separation and Western blot analysis were performed on isolated protein samples using αAHR.

levels (Fig. 4B). To verify that the interaction was not unique to Hepa1c1c7 cells, co-immunoprecipitation experiments were performed in the AHR expressing murine B cell lymphoma, CH12.LX line. Once again, the AHR/ATP5α1 interaction was observed, this time in a mouse immune cell line (Fig. 4C).

AHR mitochondrial localization

As discussed above, ATP5α1 functions as part of the multisubunit ATP synthase, raising the possibility that a portion of the cellular pool of AHR may localize to the mitochondria. To investigate this possibility, cellular fractionation studies were performed. Indeed, the AHR co-purified with the mitochondrial-specific protein cytochrome c oxidase IV (COX IV), suggesting that a fraction of the cellular AHR pool resides in the mitochondria (Fig. 5A). TCDD treatment (10 nM, 120 min) appeared to diminish the amount of AHR localized to the mitochondrial compartment; however, this decrease is concomitant with a decrease in the total cellular amount of the receptor (Fig. 5A). Mitochondrial localization of the AHR was also observed in CH12LX cells (Fig. 5B). In both cases, ATP5α1 was predominantly identified in the mitochondria with a modest amount present in the cytoplasmic fraction. Additional confirmatory experiments were performed on cellular fractionations from livers of C57BL/6 mice. These liver-derived cellular fractions similarly showed that a portion of the cellular AHR pool was in the mitochondria, and with a small fraction of ATP5α1 present in the cytoplasm (Fig. 5C). To rule out the possibility that binding of the AHR occurred nonspecifically to the outer mitochondrial membrane mitoplasts were prepared (Fig. 5D). These experiments demonstrated the presence of AHR in the mitoplast fraction. Finally, isolated mitochondria were analyzed by immunohistochemistry using anti-AHR and anti-ATP5α1 specific antibodies and demonstrated a colocalization of the two proteins in the purified organelle (Fig. 5E). Collectively, these data strongly suggest that a portion of the cellular pool of AHR is localized to the matrix of the mitochondria, the same compartment in which ATP5α1 is most abundant.

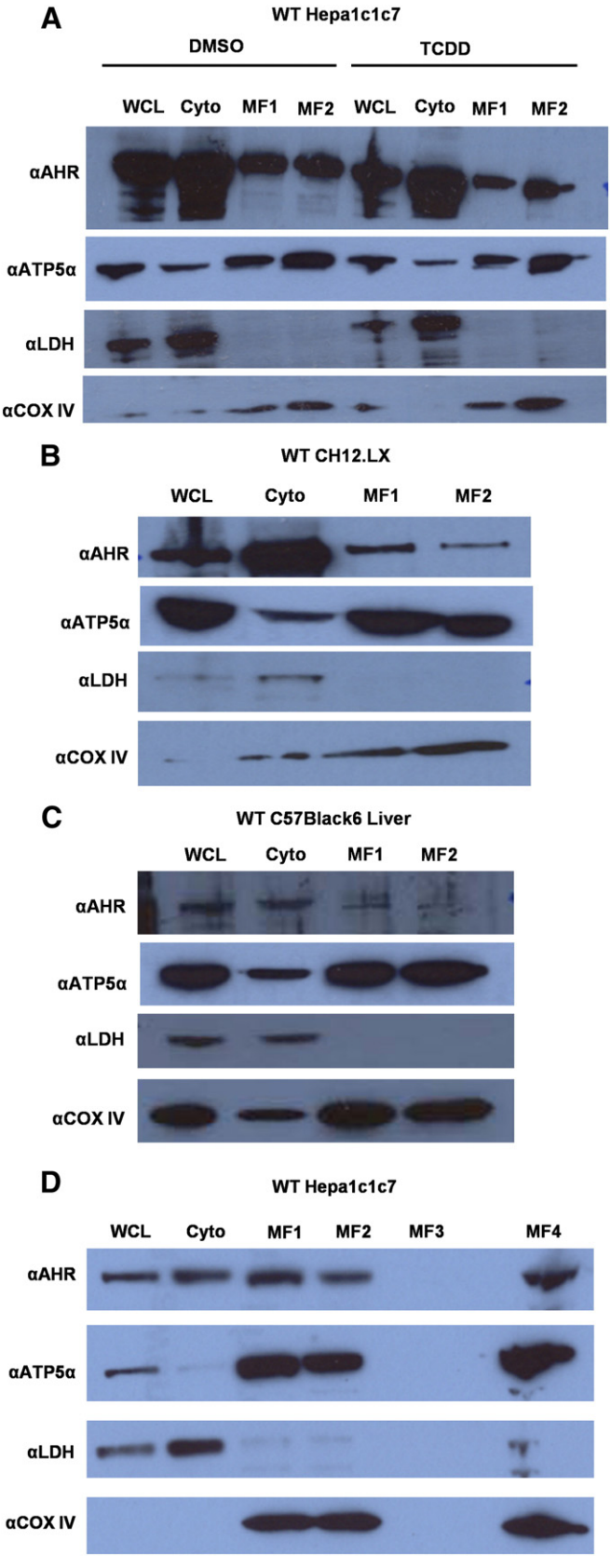

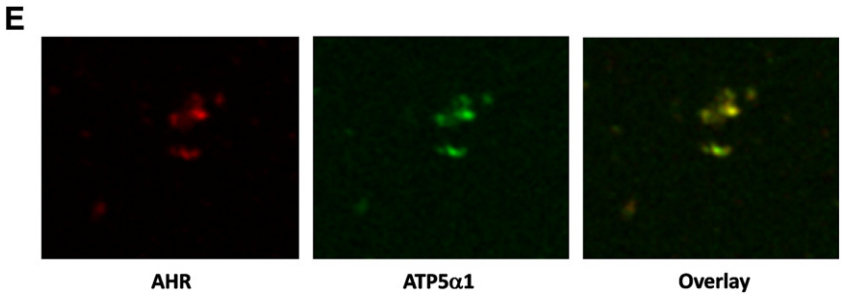

Fig. 5 Cell fractionation was performed on WT Hepa1c1c7 exposed to DMSO or TCDD (10 nM, 120 min) (A), CH12LX cells (B), or samples from a C57Bl/6 mouse liver (C). Whole cell lysates (WCL), cytosolic (Cyto), crude mitochondrial (MF1), pure mitochondrial (MF2), mitochondrial inner membrane space (MF3), and mitoplast (MF4) fractions were prepared as described in materials and methods section Mitoplast were prepared from naive WT Hepa1c1c7 (D). Cellular fractionation samples were analyzed by Western blot using antibodies specific to the AHR (top panel), ATP5α1 (second panel from top), lactate dehydrogenase (LDH, third panel from top), and Cytochrome C oxidase subunit IV (COXIV, bottom panel). Immunofluorescence imaging on isolated mitochondria using an AHR specific antibody (left panel), and an ATP5α1 specific antibody (center panel) shows AHR and ATP5α1 localization to the isolated organelles and an overlay image (right panel) shows the two proteins co-localized in the isolated organelles (E).

AHR influence on mitochondrial function

To investigate the functional relevance of AHR:ATP5α1 protein interactions, the mitochondrial inner membrane potential was indirectly measured using tetramethylrhodamine methyl ester (TMRM) by flow cytometry in several cell lines which differed in AHR expression levels. Comparison of murine B cell lymphoma lines, CH12.LX ($AHR^{+/+}$) and BCL1 ($AHR^{-/-}$) cells revealed a concentration-dependent hyperpolarization of the mitochondrial inner membrane in CH12.LX cells with TCDD treatment, when compared to the vehicle control (Fig. 6A). In contrast, BCL1 cells demonstrated a basal inner membrane polarization that was 1.5-fold higher in magnitude compared to the basal level observed in CH12.LX cells but only exhibited a modest hypopolarization of the inner membrane with TCDD treatment (Fig. 6B). Additional experiments were conducted to investigate the influence transcription may have on the AHR-dependent TCDD-induced hyperpolarization of the mitochondrial inner membrane by pretreatment of CH12.LX cells with mitomycin C. A comparable level of hyperpolarization of the inner membrane was also observed, in the presence of mitomycin C; approximately 3.5–4 fold with 30 nM TCDD treated. These results show that TCDD-mediate mitochondrial hyperpolarization occurs independently of AHR-mediated transcription (Fig. 6C).

Because CH12.LX and BCL1 cells do not share a common parental lineage, similar experiments were performed in the genetically related Hepa1c1c7 ($AHR^{+/+}$) and HepaC12 (AHR deficient) cell lines (Van Gurp and Hankinson, 1984). Initially, the level of AHR in the Hepa1c1c7 and HepaC12 was confirmed by Western blot. The HepaC12 cells express negligible amount of AHR compared to Hepa1c1c7 (Fig. 7A). TCDD induced a significant hyperpolarization of the mitochondrial inner membrane in the Hepa1c1c7 cells, similar to the CH12.LX cells. In contrast, the HepaC12 cell line showed no change in inner membrane potential when treated with TCDD (Fig. 7B and C). These results further support that TCDD-induced hyperpolarization is an AHR-dependent event. It is noteworthy that siRNA experiments were also performed to knockdown AHR in the Hepa1c1c7 cells to confirm AHR dependence. Although a significant and reproducible AHR knockdown could be achieved, the transfected cells displayed little or no TCDD-induced hyperpolarization. The mock transfected cells (i.e. lipofectamine alone) and siRNA control (scrambled sequence) also displayed no TCDD-inducible hyperpolarization, demonstrating that the transfection reagent alone disrupts mitochondrial function. This result is not surprising since the function of lipofectamine is to make membranes more fluid and permeable, in this case disrupting the mitochondrial membrane as well.

To evaluate the effect of the inner membrane hyperpolarization on cellular energetics, ATP levels were also examined. In the CH12.LX cells, only a statistically insignificant moderate decrease in ATP levels was detected upon TCDD (30 nM, 6 h) treatment (Fig. 8). The same decrease was also observed in the vehicle treated cells. Given that TCDD induces a dissociation of the AHR from ATP5α1 and a hyperpolarization of the inner membrane in the absence of a measurable change in ATP, it is hypothesized that the change in membrane potential serves to maintain ATP levels following a decrease in ATP synthase efficiency upon loss of AHR interaction.

Discussion

The xenobiotic-induced toxicities mediated through the AHR are complex in their species- and tissues-specific effects. The underlying mechanisms for these toxicities remain poorly defined and may be due, in part, to a lack of a global understanding of the role the AHR plays in different cellular processes, such as gene regulation, protein interactions, and cellular energetics. To date, investigations of the AHR have described numerous aspects of the receptor's function in both xenobiotic response and development. Moreover, it has been shown, using nuclear localization signal (NLS) and DNA binding domain (DBD) mutant mice that normal cellular trafficking is necessary but not sufficient for TCDD-induced biological responses (Bunger et al., 2003, 2008). These results support the classic view that most TCDD-induced toxicities involve AHR nuclear translocation and transcription; however, they do not rule out the possibility that other AHR-interacting proteins play important roles in the process (Blankenship and Matsumura, 1997; Ge and Elferink, 1998; Chan et al., 1999; Puga et al., 2000). Introduction of mutations to the AHR have provided important new tools to begin to define and dissect the endogenous role for this receptor. For example, cellular localization of the DBD mutant AHR is constitutively nuclear, while mutations in the NLS disrupt normal compartmental trafficking of the AHR (Bunger et al., 2003, 2008). Similarly, the triple cytochrome p450 knockout mouse displays aberrant bioavailability of the xenobiotics that influence the AHR's normal cellular signaling (Dragin et al., 2008). These recent findings are important but do not directly address, nor rule out, the possibility of secondary effects mediated by AHR protein interaction in xenobiotic-induced toxicity. Therefore, the present investigation sought to identify novel AHR interacting proteins and correlate their function to changes in TCDD-induced toxicity.

The findings reported here demonstrate a novel and intriguing link between the AHR and the mitochondrial machinery responsible for cellular energy production. The mitochondrial ATP synthase is a multi-subunit complex, localized to the inner mitochondrial membrane. ATP5α1 is one of the proteins that comprise the soluble catalytic F1 subunit of this complex. Changes in ATP5α1 levels have been linked to various disease processes, including cancer, and to play a role in tumor

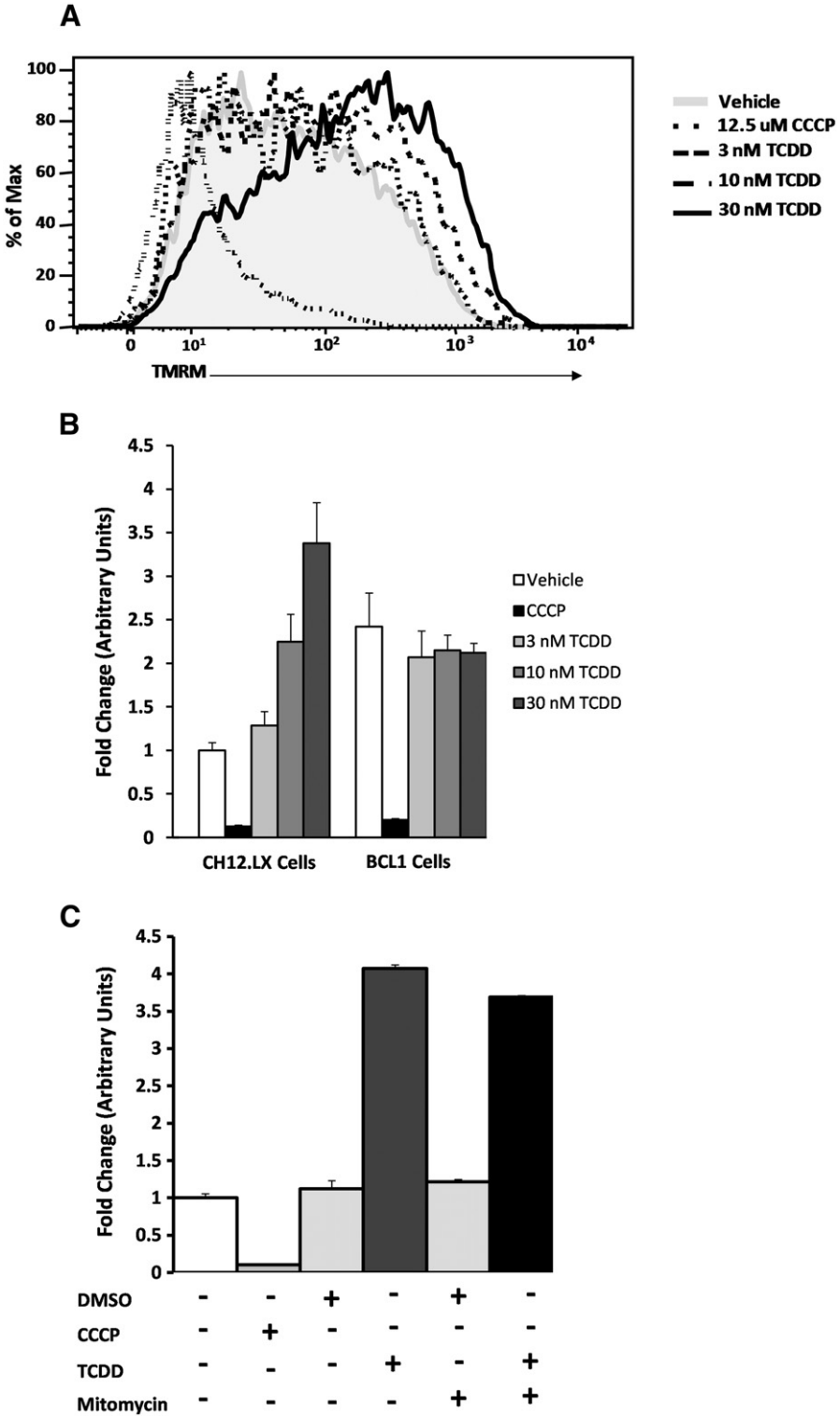

Fig. 6. Flow cytometric analysis of mitochondrial membrane potential was performed on CH12.LX (AHR+/+) cell lines exposed to DMSO (0.01% vehicle control) or TCDD (3, 10, and 30 nM) for 6 h. TMRM intensity showed a concentration dependent shift to the right when compared to vehicle control (Shaded portion) (A). Hyperpolarization was only observed in the CH12.LX cells ($AHR^{+/+}$) and not observed in the BCL1 cell line, an $AHR^{-/-}$ murine B cell line. CCCP was used as a positive control, showing effect of electron transport chain uncoupling on membrane polarization. The values were normalized to the DMSO treated CH12.LX signal (B). The hyperpolarization was not dependent upon AHR-mediated transcription as it was observed in both the presence and absence of the transcriptional inhibitor, mitomycin C. Again, CCCP was used as a positive control and the values were normalized to DMSO treated control (C).

progression and the Warburg effect (Baran et al., 2007; Seth et al., 2009; Pennington et al., 2010; Yusenko et al., 2010). The characterization of the interaction between the AHR and ATP5α1 and subsequent changes in mitochondrial function might link these observations with TCDD-induced tumor promotion (Ray and Swanson, 2009). More importantly, the AHR:ATP5α1 interaction might explain previous observations linking TCDD exposure with changes in mitochondrial function and gene expression (Senft et al., 2002; Paajarvi et al., 2005; Aly and

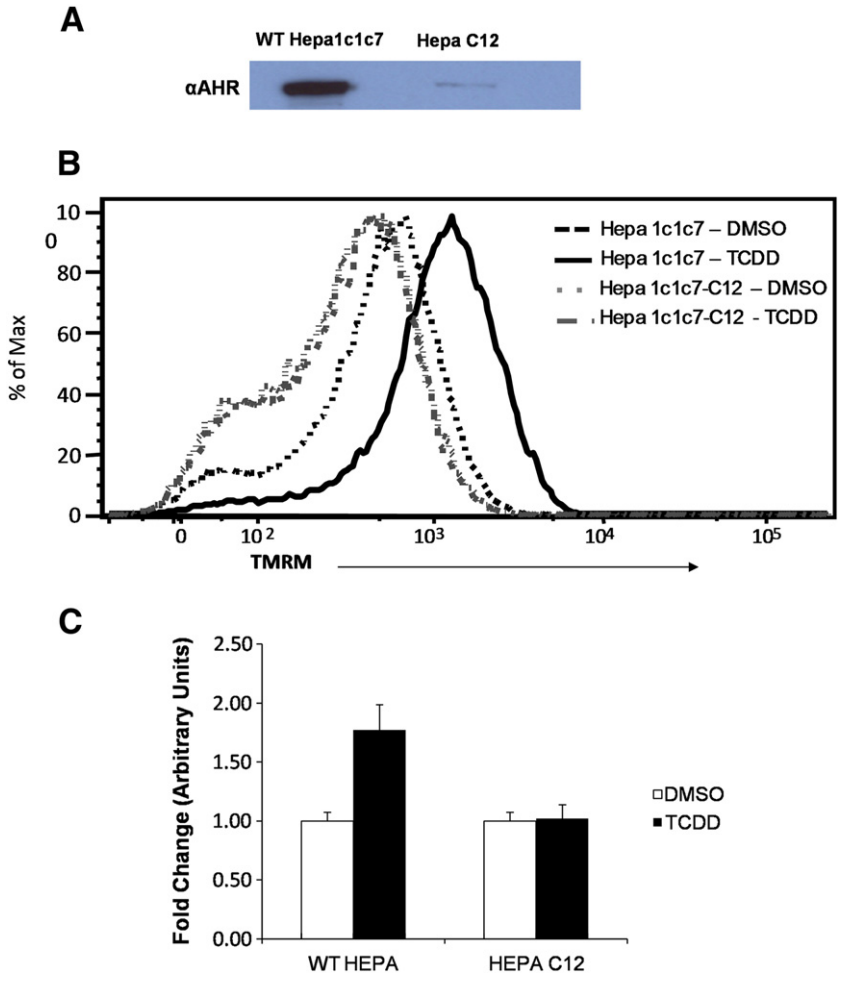

Fig. 7. Equal amounts of whole cell lysate from Hepa1c1c7 and Hepa C12 cell lines were examined for AHR expression levels by Western blotting (A) Flow cytometric analysis of mitochondrial membrane potential was performed on Hepa1c1c7 ($AHR^{+/+}$) and Hepa C12 (AHR deficient) cell lines exposed to DMSO (0.01% vehicle control) or TCDD (30 nM) for 6 h. TMRM intensity showed a TCDD-induced shift to the right when compared to vehicle control in the Hepa1c1c7 cell line. This shift was not observed in the HepaC12 (AHR deficient) cell line (B). The TMRM signal represented in B was normalized to the MitoTraker Green (MTG) signal to confirm that the increased TMRM signal was not dependent upon increased mitochondrial number and further show it was AHR dependent. The values were normalized to DMSO treated Hepa1c1c7 signal (C).

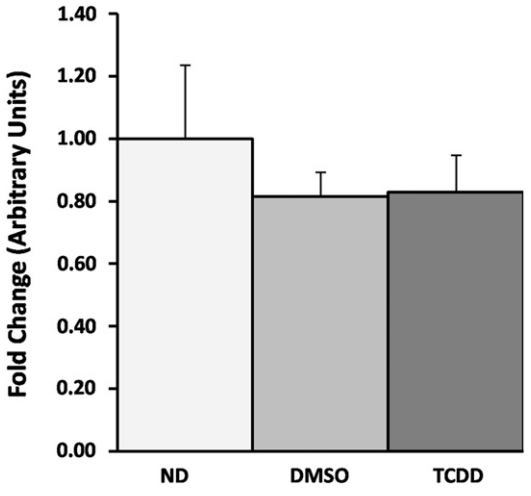

Fig. 8. To determine the influence of the mitochondrial inner membrane hyperpolarization on cellular energy, the levels of ATP were examined in CH12.LX cells. Cellular ATP was measured in naïve, DMSO (0.01% vehicle control), and TCDD (30 nM) dosed CH12.Lx cells using a luciferase reporter assay. Data were normalized to cell number and the ATP levels of the no dosed (ND) were set to 1. No significant differences were observed between the groups (D).

Domenech, 2009; Shertzer et al., 2009; Forgacs et al., 2010). For example, Senft and colleagues observed an AHR-dependent increase in TCDD-induced H_2O_2 and superoxide production that was independent of Cyp1a1 and Cyp1a2 (Senft et al., 2002). In contrast to the observed TCDD-mediated hyperpolarization in CH12.LX and Hepa1c1c7 cells, several reports have described a TCDD-induced decrease in mitochondrial membrane polarization (Paajarvi et al., 2005; Aly and Domenech, 2009). Presently the reasons for these disparate results are unclear but might be attributable to cell type specific and methodological reasons. Finally, it is tempting to speculate that AHR:ATP5α1 interactions play a broader role in TCDD-induced metabolic syndrome (Uemura et al., 2009). For example, the TCDD-induced dissociation of the AHR from the ATP synthase complex might negatively impact its enzymatic efficiency and lead to mitochondrial stress. The ensuing mitochondrial stress could play a role in the metabolic dysfunction observed following TCDD exposure. Shertzer et al. also observed that hepatocytes from TCDD-treated mice displayed a mitochondrial membrane hyperpolarization and suggested that this was due to a defect in ATP synthase (Shertzer et al., 2006). The mitochondrial-localized AHR might play an important role in cellular energetic by maintaining ATP synthase efficiency and TCDD exposure disrupts this function, leading to mitochondrial stress.

Localization of the AHR to the mitochondria is a novel finding and worthy of examination. Though the receptor itself has not previously

been associated with the mitochondria, its cytosolic partners have been. The ARA9 has been reported to aid in mitochondrial transport through interaction with TOM20 and Hsc70 (Yano et al., 2003) (MacKenzie and Payne, 2007). In support of this we have identified Hsp8, the murine homolog of Hsc70, in both AHR-TAP and ARA9-TAP MS data sets (data not shown). Hsp90 and Hsc70 have also been reported to facilitate mitochondrial transport through interaction with TOM70 (Young et al., 2003). Hsp90, itself, localizes to the mitochondria in tumor cells and influence the organelle's function (Kang et al., 2007). Finally, Hsp90 has been demonstrated to facilitate the mitochondrial import of proteins lacking traditional mitochondrial localization sequences (MLS), (Budas et al., 2010; Young et al., 2003; Halestrap, 2006). Therefore, even though the AHR lacks a recognized MLS, its cytoplasmic partners (i.e. Hsp90 and ARA9) provide a possible mechanism by which the receptor is capable of translocating to the mitochondria. Finally, the possibility that the AHR: ATP5α1 interaction is mediated through an interaction with the Hsp90 and/or ARA9 must also be considered. Though this possibility has not been tested, directly, ATP5α1 was only observed in a single TAP-ARA9 experiment (data not shown). In contrast, it was observed in multiple TAP/MS runs for the AHR.

Taken together, the data presented here suggest a direct role for the AHR in mitochondrial function and cellular energy production. However, it is important to emphasize that this role played by the AHR within the mitochondrial compartment must not be essential for the organelle's function, at least in mice, since targeted deletion of AHR is not lethal. Here we also observed that treatment with TCDD led to a hyperpolarization of the inner membrane which occurred in a transcriptionally-independent manner. This hyperpolarization concordantly occurred with a possible decrease in the amount of AHR in the mitochondria. In light of these observations, we propose that the hyperpolarization of the inner membrane occurs in response to decreased efficiency of the ATP synthase complex and that this inefficiency is a result of the reduced interaction between the AHR and the ATP synthase complex. This model is supported by the observation that the AHR deficient BCL1 cells have a resting membrane potential that is measurably higher than the AHR expressing CH12LX cells. Interestingly, and perhaps only coincidental, CH12.LX cells express remarkably high levels of AHR and exhibit a very rapid doubling rate, approximately every 12–14 h. In contrast, the BCL-1 cells exhibit a remarkably slow doubling rate, approximately every 24–28 h. The HepaC12 cells did not exhibit the same higher resting membrane potential as the BCL-1 cell line; however, the doubling time for the Hepa C12 cell line is comparable to the BCL-1 cell line. Though the results presented here do not rule out a role for the AHR in cell cycle control, it is interesting to speculate that these doubling times are influenced by the putative decrease in ATP synthase efficiency following loss of the receptor. Finally, the discovery of a role for the AHR in cellular energy production establishes a possible mechanism by which dioxin-induced toxic endpoints such as wasting syndrome or immune system suppression may be occurring.

Conflict of interest statement

The authors declare that there are no conflicts of interest.

Acknowledgments

We would like to thank Drs Christopher Bradfield and Garry Nolan for their willingness to share cell lines and reagents. This work was supported by NIH grant P42 ES04911.

References

Aly, H.A., Domenech, O., 2009. Cytotoxicity and mitochondrial dysfunction of 2,3,7,8-tetrachlorodibenzo-p-dioxin (TCDD) in isolated rat hepatocytes. Toxicol. Lett. 191, 79–87.

Arnold, L.W., LoCascio, N.J., Lutz, P.M., Pennell, C.A., Klapper, D., Haughton, G., 1983. Antigen-induced lymphomagenesis: identification of a murine B cell lymphoma with known antigen specificity. J. Immunol. 131, 2064–2068.

Baran, A.A., Silverman, K.A., Zeskand, J., Koratkar, R., Palmer, A., McCullen, K., Curran Jr., W.J., Edmonston, T.B., Siracusa, L.D., Buchberg, A.M., 2007. The modifier of Min 2 (Mom2) locus: embryonic lethality of a mutation in the Atp5a1 gene suggests a novel mechanism of polyp suppression. Genome Res. 17, 566–576.

Barhoover, M.A., Hall, J.M., Greenlee, W.F., Thomas, R.S., 2009. Aryl hydrocarbon receptor regulates cell cycle progression in human breast cancer cells via a functional interaction with cyclin-dependent kinase 4. Mol. Pharmacol. 77, 195–201.

Bishop, G.A., Haughton, G., 1986. Induced differentiation of a transformed clone of Ly-1 + B cells by clonal T cells and antigen. P. Natl. Acad. Sci. USA 83, 7410–7414.

Blankenship, A., Matsumura, F., 1997. 2,3,7,8-Tetrachlorodibenzo-p-dioxin-induced activation of a protein tyrosine kinase, pp 60src, in murine hepatic cytosol using a cell-free system. Mol. Pharmacol. 52, 667–675.

Bradfield, C.A., Poland, A., 1988. A competitive binding assay for 2,3,7,8-tetrachlorodibenzo-p-dioxin and related ligands of the Ah receptor. Mol. Pharmacol. 34, 682–688.

Budas, G. R., Churchill, E. N., Disatnik, M. H., Sun, L., and Mochly-Rosen, D., 2010. Mitochondrial import of PKCepsilon is mediated by HSP90: a role in cardioprotection from ischaemia and reperfusion injury. *Cardiovasc Res* **88**, 83–92.

Bunger, M.K., Moran, S.M., Glover, E., Thomae, T.L., Lahvis, G.P., Lin, B.C., Bradfield, C.A., 2003. Resistance to 2,3,7,8-tetrachlorodibenzo-p-dioxin toxicity and abnormal liver development in mice carrying a mutation in the nuclear localization sequence of the aryl hydrocarbon receptor 10.1074/jbc.M209594200. J. Biol. Chem. 278, 17767–17774.

Bunger, M.K., Glover, E., Moran, S.M., Walisser, J.A., Lahvis, G.P., Hsu, E.L., Bradfield, C.A., 2008. Abnormal liver development and resistance to 2,3,7,8-tetrachlorodibenzo-p-dioxin toxicity in mice carrying a mutation in the DNA-binding domain of the aryl hydrocarbon receptor. Toxicol. Sci. 106, 83–92.

Carver, L.A., LaPres, J.J., Jain, S., Dunham, E.E., Bradfield, C.A., 1998. Characterization of the Ah receptor-associated protein, ARA9. J. Biol. Chem. 273, 33580–33587.

Chan, W.K., Yao, G., Gu, Y.Z., Bradfield, C.A., 1999. Cross-talk between the aryl hydrocarbon receptor and hypoxia inducible factor signaling pathways. Demonstration of competition and compensation. J. Biol. Chem. 274, 12115–12123.

Daum, G., Gasser, S.M., Schatz, G., 1982. Import of proteins into mitochondria. Energy-dependent, two-step processing of the intermembrane space enzyme cytochrome b2 by isolated yeast mitochondria. J. Biol. Chem. 257, 13075–13080.

Denison, M.S., Fisher, J.M., Whitlock Jr., J.P., 1988. The DNA recognition site for the dioxin-Ah receptor complex. Nucleotide sequence and functional analysis. J. Biol. Chem. 263, 17221–17224.

Dragin, N., Shi, Z., Madan, R., Karp, C.L., Sartor, M.A., Chen, C., Gonzalez, F.J., Nebert, D.W., 2008. Phenotype of the Cyp1a1/1a2/1b1$^{-/-}$ triple-knockout mouse. Mol. Pharmacol. 73, 1844–1856.

Forgacs, A.L., Burgoon, L.D., Lynn, S.G., LaPres, J.J., Zacharewski, T., 2010. Effects of TCDD on the expression of nuclear encoded mitochondrial genes. Toxicol. Appl. Pharmacol. 246, 58–65.

Fujisawa-Sehara, A., Sogawa, K., Yamane, M., Fujii-Kuriyama, Y., 1987. Characterization of xenobiotic responsive elements upstream from the drug-metabolizing cytochrome P-450c gene: a similarity to glucocorticoid regulatory elements. Nucleic Acids Res. 15, 4179–4191.

Ge, N.-L., Elferink, C.J., 1998. A direct interaction between the aryl hydrocarbon receptor and retinoblastoma protein. Linking dioxin signaling to the cell cycle. J. Biol. Chem. 273, 22708–22713.

Halestrap, A.P., 2006. Mitochondria and preconditioning: a connexin connection? Circ. Res. 99, 10–12.

Kang, B.H., Plescia, J., Dohi, T., Rosa, J., Doxsey, S.J., Altieri, D.C., 2007. Regulation of tumor cell mitochondrial homeostasis by an organelle-specific Hsp90 chaperone network. Cell 131, 257–270.

Kearney, P.C., Woolson, E.A., Isensee, A.R., Helling, C.S., 1973. Tetrachlorodibenzodioxin in the environment: sources, fate, and decontamination. Environ Health Perspect. 5, 273–277.

Lee, K., Burgoon, L.D., Gier, L.E., Dere, E., Zacharewski, T.R., Hogenesch, J.B., LaPres, J.J., 2006. Identification and characterization of genes susceptible to transcriptional cross-talk between the hypoxia and dioxin signaling cascades. Chem. Res. Toxicol. 1284–1293.

Lowry, O.H., Rosebrough, N.J., Farr, A.L., Randall, R.J., 1951. Protein measurement with the Folin phenol reagent. J. Biol. Chem. 193, 265–275.

MacKenzie, J.A., Payne, R.M., 2007. Mitochondrial protein import and human health and disease. Biochim. Biophys. Acta 1772, 509–523.

Mandal, P.K., 2005. Dioxin: a review of its environmental effects and its aryl hydrocarbon receptor biology. J. Comp. Physiol. B 175, 221–230.

Paajarvi, G., Viluksela, M., Pohjanvirta, R., Stenius, U., Hogberg, J., 2005. TCDD activates Mdm2 and attenuates the p53 response to DNA damaging agents. Carcinogenesis 26, 201–208.

Pennington, K., Peng, J., Hung, C.C., Banks, R.E., Robinson, P.A., 2010. Differential effects of wild-type and A53T mutant isoform of alpha-synuclein on the mitochondrial proteome of differentiated SH-SY5Y cells. J. Proteome Res. 9, 2390–2401.

Perdew, G.H., 1988. Association of the Ah receptor with the 90-kDa heat shock protein. J. Biol. Chem. 263, 13802–13805.

Poland, A., Glover, E., 1977. Chlorinated biphenyl induction of aryl hydrocarbon hydroxylase activity: a study of the structure activity relationship. Mol. Pharmacol. 13, 924.

Poland, A., Glover, E., 1980. 2,3,7,8-Tetrachlorodibenzo-*p*-dioxin: segregation of toxicity with the *Ah* locus. Mol. Pharm. 17, 86–94.

Poland, A., Kende, A., 1977. The genetic expression of aryl hydrocarbon hydroxylase activity: evidence for a receptor mutation in nonresponsive mice. Cold Spring Harbor Lab. 847–867.

Poland, A., Knutson, J.C., 1982. 2,3,7,8-tetrachlorodibenzo-p-dioxin and related halogenated aromatic hydrocarbons: examination of the mechanism of toxicity. Annu. Rev. Pharmacol. 22, 517–554.
Poland, A., Glover, E., Kende, A.S., 1976. Stereospecific, high affinity binding of 2,3,7,8-tetrachlorodibenzo-p-dioxin by hepatic cytosol. Evidence that the binding species is receptor for induction of aryl hydrocarbon hydroxylase. J. Biol. Chem. 251, 4936–4946.
Poland, A., Greenlee, W.F., Kende, A.S., 1979. Studies on the mechanism of action of the chlorinated dibenzo-p-dioxins and related compounds. Ann. N.Y. Acad. Sci. 320, 214–230.
Prokipcak, R.D., Denison, M.S., Okey, A.B., 1990. Nuclear Ah receptor from mouse hepatoma cells: effect of partial proteolysis on relative molecular mass and DNA-binding properties. Arch. Biochem. Biophys. 283, 476–483.
Puga, A., Barnes, S.J., Dalton, T.P., Chang, C., Knudsen, E.S., Maier, M.A., 2000. Aromatic hydrocarbon receptor interaction with the retinoblastoma protein potentiates repression of E2F-dependent transcription and cell cycle arrest. J. Biol. Chem. 275, 2943–2950.
Ray, S., Swanson, H.I., 2009. Activation of the aryl hydrocarbon receptor by TCDD inhibits senescence: a tumor promoting event? Biochem. Pharmacol. 77, 681–688.
Schmidt, J.V., Bradfield, C.A., 1996. AH receptor signaling pathways. Annu. Rev Cell. Dev. Bi. 12, 55–89.
Senft, A.P., Dalton, T.P., Nebert, D.W., Genter, M.B., Puga, A., Hutchinson, R.J., Kerzee, J.K., Uno, S., Shertzer, H.G., 2002. Mitochondrial reactive oxygen production is dependent on the aromatic hydrocarbon receptor. Free Radic. Biol. Med. 33, 1268–1278.
Seth, R., Keeley, J., Abu-Ali, G., Crook, S., Jackson, D., Ilyas, M., 2009. The putative tumour modifier gene ATP5A1 is not mutated in human colorectal cancer cell lines but expression levels correlate with TP53 mutations and chromosomal instability. J. Clin. Pathol. 62, 598–603.
Shertzer, H.G., Genter, M.B., Shen, D., Nebert, D.W., Chen, Y., Dalton, T.P., 2006. TCDD decreases ATP levels and increases reactive oxygen production through changes in mitochondrial F(0)F(1)-ATP synthase and ubiquinone. Toxicol. Appl. Pharmacol. 217, 363–374.
Shertzer, H.G., Schneider, S.N., Kendig, E.L., Clegg, D.J., D'Alessio, D.A., Johansson, E., Genter, M.B., 2009. Tetrahydroindenoindole inhibits the progression of diabetes in mice. Chem. Biol. Interact. 177, 71–80.
Shevchenko, A., Wilm, M., Vorm, O., Mann, M., 1996. Mass spectrometric sequencing of proteins silver-stained polyacrylamide gels. Anal. Chem. 68, 850–858.
Slavin, S., Strober, S., 1978. Spontaneous murine B-cell leukaemia. Nature 272, 624–626.
Tian, Y., Rabson, A.B., Gallo, M.A., 2002. Ah receptor and NF-[kappa]B interactions: mechanisms and physiological implications. Chem. Biol. Interact. 141, 97–115.
Uemura, H., Arisawa, K., Hiyoshi, M., Kitayama, A., Takami, H., Sawachika, F., Dakeshita, S., Nii, K., Satoh, H., Sumiyoshi, Y., Morinaga, K., Kodama, K., Suzuki, T., Nagai, M., 2009. Prevalence of metabolic syndrome associated with body burden levels of dioxin and related compounds among Japan's general population. Environ Health Perspect. 117, 568–573.
Van Gurp, J.R., Hankinson, O., 1984. Isolation and characterization of revertants from four different classes of aryl hydrocarbon hydroxylase-deficient hepa-1 mutants. Mol. Cell. Biol. 4, 1597–1604.
Vengellur, A., LaPres, J.J., 2004. The role of hypoxia inducible factor 1{alpha} in cobalt chloride induced cell death in mouse embryonic fibroblasts. Toxicol. Sci. 82, 638–646.
Yano, M., Terada, K., Mori, M., 2003. AIP is a mitochondrial import mediator that binds to both import receptor Tom20 and preproteins. J. Cell Biol. 163, 45–56.
Young, J.C., Hoogenraad, N.J., Hartl, F.U., 2003. Molecular chaperones Hsp90 and Hsp70 deliver preproteins to the mitochondrial import receptor Tom70. Cell 112, 41–50.
Yusenko, M.V., Ruppert, T., Kovacs, G., 2010. Analysis of differentially expressed mitochondrial proteins in chromophobe renal cell carcinomas and renal oncocytomas by 2-D gel electrophoresis. Int. J. Biol. Sci. 6, 213–224.